AFRL-AFOSR-VA-TR-2019-0360

Spectroscopic studies of NdO+ in support of atmospheric release probes of the ionosphere

Michael C Heaven
EMORY UNIVERSITY

11/22/2019
Final Report

Air Force Research Laboratory
AF Office Of Scientific Research (AFOSR)/ RTB2
Arlington, Virginia 22203
Air Force Materiel Command

REPORT DOCUMENTATION PAGE

Form Approved
OMB No. 0704-0188

1. REPORT DATE *(DD-MM-YYYY)*	2. REPORT TYPE	3. DATES COVERED *(From - To)*
22-11-2019	Final Performance	01 May 2018 to 30 Oct 2019

4. TITLE AND SUBTITLE
Spectroscopic studies of NdO+ in support of atmospheric release probes of the ionosphere

5a. CONTRACT NUMBER

5b. GRANT NUMBER
FA9550-18-1-0414

5c. PROGRAM ELEMENT NUMBER
61102F

6. AUTHOR(S)
Michael C Heaven

5d. PROJECT NUMBER

5e. TASK NUMBER

5f. WORK UNIT NUMBER

7. PERFORMING ORGANIZATION NAME(S) AND ADDRESS(ES)
EMORY UNIVERSITY
201 DOWMAN DR
ATLANTA, GA 30322-1018 US

8. PERFORMING ORGANIZATION REPORT NUMBER

9. SPONSORING/MONITORING AGENCY NAME(S) AND ADDRESS(ES)
AF Office of Scientific Research
875 N. Randolph St. Room 3112
Arlington, VA 22203

10. SPONSOR/MONITOR'S ACRONYM(S)
AFRL/AFOSR RTB2

11. SPONSOR/MONITOR'S REPORT NUMBER(S)
AFRL-AFOSR-VA-TR-2019-0360

12. DISTRIBUTION/AVAILABILITY STATEMENT
A DISTRIBUTION UNLIMITED: PB Public Release

13. SUPPLEMENTARY NOTES

14. ABSTRACT
The Air Force Research Laboratory (AFRL) is interested in using an artificial increase in electron density to control radio and microwave opacity in the thermosphere. One strategy for achieving this condition is to use exothermic metal-based chemiionization reactions of the form M + O -> (MO+) + e as the source of free electrons. Attention has been focused on atmospheric release of Sm and Nd atomic vapors at high altitude (>100 km) by sounding rockets. An unexpectedly low yield of SmO+ led to the conclusion that the Sm+O-> (SmO+) + e reaction is almost thermoneutral. This discovery motivated new studies of the thermochemistry of the Nd+O-> (NdO+) + e reaction. Key parameters for the determination of thermodynamics are the molecular ionization energy and the density of low-lying electronically excited states of the NdO+ ion. The primary goal of this research effort was to measure the ionization energy of NdO and characterize the lower energy states of NdO+ by means of two-color photoionization spectroscopy. The value obtained for the ionization energy, 5.5083(2) eV, was 0.54 eV higher than previous estimates. Combined with a new determination of the bond energy for NdO+ (Ghiassee et al. J. Chem. Phys. 150, 144309 (2019)) this leads to the conclusion that the chemi-ionization reaction is exothermic by 1.76(10) eV, and promising for future atmospheric release experiments. The spectroscopic measurements for NdO+ have revealed thirty vibronic levels that arise from eight electronic states. Spectra were observed for these states at the level of rotational structure resolution. The energy level pattern and supporting electronic structure calculations indicated that all of the observed states correlated with the Nd(4f3, 4I)O+ configuration. The structure was consistent with a ligand field theory model where the electronic states of the Nd3+(4f3, 4I) atomic ion define a repeat

15. SUBJECT TERMS
Neodymium oxide

16. SECURITY CLASSIFICATION OF:			17. LIMITATION OF ABSTRACT	18. NUMBER OF PAGES	19a. NAME OF RESPONSIBLE PERSON
a. REPORT	b. ABSTRACT	c. THIS PAGE			BERMAN, MICHAEL
Unclassified	Unclassified	Unclassified	UU		19b. TELEPHONE NUMBER *(Include area code)* 703-696-7781

Standard Form 298 (Rev. 8/98)
Prescribed by ANSI Std. Z39.18

Low energy states of NdO^+ probed by photoelectron spectroscopy

Robert A. VanGundy, Thomas D. Persinger and Michael C. Heaven

Department of Chemistry, Emory University, Atlanta, GA 30322

Abstract

The ionization energy (IE) of NdO and the low-energy electronic states of NdO^+ have been examined by means of two-color photoionization spectroscopy. The value obtained for the IE, 5.5083(2) eV is 0.54 eV higher than previous estimates. This leads to the conclusion that the auto-ionization reaction $Nd + O \rightarrow NdO^+ + e^-$ is exothermic by 1.76(10) eV.

Thirty vibronic levels of NdO^+ arising from eight electronic states were observed with partial rotational resolution. The energy level pattern and supporting electronic structure calculations indicated that all of the observed states correlated with the $Nd^{3+}(4f^3, {}^4I)O^{2-}$ configuration. The structure was consistent with a ligand field theory model where the electronic states of the $Nd^{3+}(4f^3, {}^4I)$ atomic ion define a repeated motif in the electronic state energy intervals of the molecular ion. Comparisons with UO^+ show close similarity in the electronic structures of these isoelectronic species.

Introduction

There were two primary motivations for the study of NdO^+ reported here. The first is associated with attempts to use metal-based chemi-ionization reactions of the form

$$M + O \rightarrow MO^+ + e \qquad (1)$$

as a means to modulate the local electron density at high altitudes (>100 km). The Air Force Research Laboratory (AFRL) is interested in using an artificial increase in electron density to control radio and microwave opacity in the thermosphere[1,2]. To date, attention has been focused on atmospheric release of Sm and Nd atomic vapors by sounding rockets[3-5]. Based on laboratory measurements, both metals were predicted to undergo associative ionization via reaction 1. Measurements of bond dissociation energies and ionization energies indicated that the reactions were exothermic by -0.33±0.10 and -2.3±0.3 eV for Sm and Nd, respectively[1]. Trials conducted using Sm yielded unexpectedly low electron densities (by a factor of 10-100)[1,6]. This prompted a reexamination of the Sm thermochemistry, where it was found that reaction 1 is almost thermoneutral (-0.08±0.07 eV)[6]. Hence, the back reaction (dissociative recombination) was partially responsible for the low electron yields.

Atmospheric release experiments for Nd were not as well-characterized as those for Sm. On the basis of emission spectroscopy and the drift direction of the emitting cloud it was concluded that the primary product was neutral NdO[1]. This was a surprising result given the expectation of a rapid exothermic reaction and the improbability of two-body Nd+O→NdO association under the low-pressure conditions of the thermosphere.

Ard et al.[1] have since examined the Sm+O and Nd+O reactions in a selected ion flow tube apparatus. At room temperature they found that the Nd+O→$NdO^+ + e$ reaction was very efficient, with a rate constant ($3x10^{-10}$ cm^3 s^{-1}) that was consistent with the hard-sphere collision

frequency. The reaction for Sm was considerably slower (~$7x10^{-12}$ cm^3 s^{-1}) and there was evidence to indicate that the reactive species was a low-lying excited state of Sm.

The metal oxide ionization energy (IE) is an important factor in the determination of the energetics of reaction 1. A significant error in the exothermicity of the Sm+O reaction was largely due to an underestimation of the SmO IE by 0.2 eV[6]. This error was probably caused by the presence of electronically excited SmO in the electron impact ionization – mass spectrometry measurements (high temperature thermal vaporization was used to generate gas phase SmO)[7]. As the IE for NdO was also obtained by this method[7], it may also be significantly underestimated (it has been experimentally confirmed that NdO has many low-lying states[8-12]). In the present work we have measured the IE of NdO using resonantly enhanced two-color photo-ionization. As the first photon excites a resonant transition that originates from the ground electronic state, this technique is not subject to errors resulting from the presence of thermally excited molecules.

The second motivation for this study concerns the low energy states of the NdO^+ cation. It is well established that lanthanide oxides (LnO) and their ions have dense manifolds of low-energy electronic states due to the presence of partially filled 4f orbitals. Ligand field theory (LFT) has proved to be very effective in predicting the manifolds of low-energy states by treating the molecule as a Ln^{2+} atomic ion perturbed by the electrostatic interaction with a closed-shell O^{2-} ligand (with the cations modeled as $Ln^{3+}O^{2-}$ systems)[13,14]. Ab initio electronic structure calculations for LnO/LnO^+ species are challenging due to the number of electrons, open 4f sub-shell, and strong relativistic effects. Consequently, comparisons between computational predictions and experimental data provide valuable tests of methodologies for treating electron correlation and both scalar and vector relativistic contributions to the energy. For NdO, LFT[14] and multi-reference ab initio calculations with relativistic corrections[15] yield reasonably good

predictions for the observed low energy states. To date, there has been no such comparison for the NdO^+ cation. A relativistic electronic structure calculation for the low energy states has been reported[16] but there are no published spectra or LFT predictions.

It is often considered that the chemical properties of the actinides and lanthanides will be similar, so that the lanthanides may be treated as surrogates for investigation of the properties of the more hazardous and unstable members of the actinide family. This approach has been valuable, but a potential point of departure is associated with differences between 4f and 5f orbitals. The lanthanide 4f orbitals are compact, atomic-like and minimally involved in chemical bonding. The situation is not so clear-cut for the early actinides, where the radial extent of the 5f orbitals is greater and the degree to which they become involved in covalent bonding is still an open question. For this reason, Krauss and Stevens[16] reported results for both NdO^+ and iso-electronic UO^+. They found that the ground and low-lying states could be correlated with the $Nd^{3+}(4f^3\ ^4I)O^{2-}$ and $U^{3+}(5f^3\ ^4I)O^{2-}$ configurations. Furthermore, the patterns of electronic states predicted for both ions were consistent with electrostatic perturbation of the metal atomic free ions. One implication was that covalent interactions of the 5f orbitals were minimal for UO^+. A subsequent experimental investigation of UO^+ confirmed these conclusions[17].

In this study we present the first spectroscopic characterization of NdO^+. To facilitate assignment of the spectra and test the capabilities of current computational models we also report the results of relativistic multi-reference configuration interaction calculations for the molecular ion. Limitations of the calculations are discussed, with further reflection on the similarities of NdO^+ and UO^+.

Spectroscopic background for NdO

The spectroscopic technique used to examine NdO^+ involved excitation of an electronic transition of neutral NdO, followed by photoionization from the excited state[18]. Consequently, some background concerning the spectroscopy of NdO facilitates description of the results. It has been established that the ground state is X(1)4, arising from the $Nd^{2+}(4f^3 6s, {}^5I)O^{2-}$ configuration[8,9,11,12,14,15]. Here we use the standard notation for low-lying electronic states of the form $(m)\Omega$, where Ω is the unsigned projection of the electronic angular momentum along the internuclear axis and m designates the energy ordering of the states for a specific value of Ω. Hence, (1)4 indicates the lowest energy state with Ω=4. The traditional alphabetic label "X" is indicated for the ground state alone. The first electronically excited state of NdO is (1)5, which is just 474 cm^{-1} above the ground state[12]. Higher energy states, for which it is usually difficult to identify the configurational parentage, are labeled as $[E]\Omega$, where E is the term energy of the state, in units of 1000 cm^{-1}. For example, we used the [11.540]3-X(1)4 transition[12] in several reported measurements. This Ω=3 excited state had a term energy of 11539.89 cm^{-1}.

Several studies of the electronic spectra of NdO have been carried out at the level of rotational resolution[8-12]. Stark and Zeeman effect measurements have been used to determine the electric dipole moment and magnetic g-factor for the X(1)4 state[11]. Electronic structure calculations have been carried out to guide the assignment of the many low energy states. LFT calculations were reported by Carette and Hocquet[14], while Allouche et al.[15] used relativistic multi-reference configuration interaction (MRCI) methods to predict the energies and molecular constants for 54 states (all with term energies below 8000 cm^{-1}).

Theoretical models for NdO^+ and UO^+

Krauss and Stevens[16] employed a restricted valence configuration interaction method to predict the low energy electronic states of NdO^+ at an internuclear distance of 1.85 Å. The basis set for Nd included a relativistic core potential and the valence basis sets for both Nd and O were of double-zeta quality. Similar calculations were carried out for UO^+ and it is helpful to consider the UO^+ results first as these have been confirmed by subsequent higher-level calculations[19] and experimental measurements[17].

The lowest energy states of UO^+ correlate with the formal $U^{3+}(5f^3; {}^4I)O^{2-}$ configuration. In the following we use J_a to designate the total electronic angular momentum of the atomic ion. In ascending energy order, the spin-orbit components of ^4I are J_a=4.5, 5.5, 6.5, and 7.5. When the O^{2-} ligand approaches, each J_a level is split into J_a+1/2 Kramers doublets that are labeled by Ω, the unsigned projection of J_a on the internuclear axis. For example, J_a=4.5 splits into the molecular ion states Ω=4.5, 3.5, 2.5, 1.5, 0.5, in ascending energy order. The ligand field is relatively weak compared to the atomic ion spin-orbit coupling interaction, such that the energy spread of the J_a=4.5, Ω=4.5 – 0.5 energy levels (1325 cm^{-1} from experiment[17]) is smaller than the U^{3+} $^4I_{5.5}$-$^4I_{4.5}$ energy interval (4265 cm^{-1})[20]. The spin-orbit coupling of the atomic ion is only slightly perturbed by the ligand field, such that the lowest energy molecular state of J_a=Ω=5.5 is 4178 cm^{-1} above J_a=Ω=4.5. The UO^+ calculations of Krauss and Stevens[16] were approximately in agreement with this weak-field model, although the ligand-field splitting was overestimated and the spin-orbit coupling was underestimated. Tyagi et al.[19] reported multi-configuration self-consistent field calculations that were closer to the experimental results and in agreement with the LFT model of the electronic structure[17,21].

Krauss and Stevens' calculations for NdO^+ predicted that the low energy states arise from the $Nd^{3+}(4f^3; {}^4I)O^{2-}$ configuration, with the lowest energy states being the J_a=4.5, Ω=4.5 – 0.5 series[16]. The calculated energy spread for these states was 904 cm^{-1}. As for UO^+, this range was appreciably smaller than the 1897 cm^{-1} ${}^4I_{5.5}$-${}^4I_{4.5}$ atomic ion interval of $Nd^{3+}(4f^3)$[22]. Since the study by Krauss and Stevens[16] the computational techniques and basis sets that can be applied for studies of NdO^+ have advanced significantly. Consequently, we have carried out multi-reference configuration interaction (MRCI) calculations for Nd^{3+} and NdO^+. The atomic ion was included as the calculations could be used to evaluate the treatment of the spin-obit coupling through comparison with accurate spectroscopic data.

The electronic structure calculations reported here were performed using the Molpro 2012 suite of programs[23]. The basis set for Nd consisted of a 28 electron relativistic core potential combined with an Atomic Natural Orbital basis set of quadruple zeta quality for the valence orbitals (ECP28MWB_ANO). The augmented, correlation consistent polarized valence triple zeta basis set (aug-cc-pvtz) was used for oxygen. Complete active space, self-consistent field (CASSCF) calculations followed by MRCI calculations were used to obtain initial energies for the spin-free excited states. The active space was defined by the Nd 4f, 5d and 6s orbitals (3 electrons in 13 orbitals). Electrons in lower energy valence orbitals were correlated, but the orbitals were constrained to be doubly occupied. For both Nd^{3+} and NdO^+ the thirteen states of $4f^3$, ${}^4I$ were calculated. The final step was inclusion of the spin-orbit interaction. The matrix elements of the spin-orbit operator were computed using the CASSCF wavefunctions, but the spin-free energies used for the diagonal elements were taken from the MRCI calculations. The results for $Nd^{3+}(4f^3, {}^4I)$ are compared with experimental data in Table 1. The spin-orbit (SO)

splitting was recovered fairly well, with an average error of 185 cm^{-1}. This was sufficient for state assignment purposes.

Optimization of the bond length for $Nd^{3+}(4f^3, {}^4I)O^{2-}$ was carried out using the CASSCF level of theory, which converged to a value of R_e=1.742 Å. Results from the MRCI-SO calculations for NdO^+ with R=1.742 Å are collected in Table 2. The structure follows the expected perturbed atomic ion model. Note that the energy spacings for the Ω=J_a levels are quite close to the values for the spin-orbit states given by the free-ion calculations (c.f., Table 1). This indicates that the spin-orbit coupling is only slightly perturbed by the ligand field. It is also apparent that the sub-levels of each J_a state give rise to a series of molecular states with Ω decreasing from J_a to 0.5 with increasing energy. The ground state is predicted to be X(1)4.5, the same as the experimentally verified assignment for UO^+[17].

Experiment

The apparatus used for these measurements has been described previously[17,18,24]. Gas phase NdO was produced using a Smalley-type pulsed laser ablation source[25]. The metal source consisted of rod of pure Nd (ESPI Metals, natural isotopic composition). The rod was ablated by the fundamental pulses (1064 nm, 5 ns duration) from a Q-switched Nd/YAG laser (Continuum Minilite II), and the ablation plume was entrained in a gas flow consisting of 1% NO in He. The gas was introduced by means of a pulsed valve (Parker General Series 9) that was synchronized with the ablation laser timing. The source pressure for the carrier gas was found to be optimal near 60 psi. To provide a fresh metal surface for each ablation pulse, the rod was continuously rotated and translated. Following entrainment of the metal vapor in the carrier gas, the mixture was expanded into a vacuum chamber through a 2 mm diameter orifice. This expansion process

typically cooled the NdO to rotational temperatures in the range of 20-40 K. The core of the supersonic expansion was sampled through a skimmer into a second chamber, where the resulting molecular beam traversed the source region of a time-of-flight mass spectrometer.

Two dye lasers were used for photoionization of NdO. Both were Nd/YAG pumped systems with pulse durations of approximately 10 ns (Lambda-Physik Scan Mate Pro, 0.15 cm^{-1} linewidth (first photon=pump) and Continuum ND6000, linewidth 0.1 cm^{-1} (second photon=probe)). Frequency doubling of the ND6000 laser was used to provide tunable radiation in the 300-370 nm wavelength range. The dye laser beams were spatially overlapped and counter-propagated along an axis that was perpendicular to the direction of the molecular beam. The dye lasers were wavelength-calibrated using a Bristol Instruments Model 821 wavemeter. Pulse timings were controlled by digital delay generators (Stanford Research Systems model D345).

Resonantly enhanced multiphoton spectroscopy (REMPI) was used to optimize production of NdO^+ for further experiments. The strongest signal for NdO^+ 1 + 1' REMPI occurred when both lasers were overlapped temporally at the exit window for the probe laser. The electric field in the ion source region of the time-of-flight mass spectrometer (TOFMS) was 364 V/cm. Seven isotopes of neodymium were present in natural abundance and the TOF-MS resolved all isotopes. The most abundant isotope ^{142}Nd (27.2%) was the primary focus for all experiments.

Photoionization efficiency (PIE) measurements were used to provide an initial estimate for the IE of NdO. The pump laser was tuned to a NdO transition and the probe laser photon energy was varied to find the threshold at which photoionization occurred. The threshold was confirmed to be a two-color process by detuning the pump photon energy from the neutral

molecule transition and observing the loss of the signal from the photon ionization caused by the probe laser.

Pulsed Field Ionization Zero Kinetic Energy photoelectron spectroscopy (PFI-ZEKE) was used to refine the IE value provided by the PIE measurement, and to further examine the NdO^+ electronic structure. In the technique employed here, the high-*n* Rydberg states were accessed via two-photon excitation of the neutral molecule. The grids of the TOFMS were reversed-biased (relative to the REMPI configuration) to facilitate electron detection. During the laser excitation sequence, the repeller plate was held at -5.1 or -5.2V and the extractor at -5V, creating an electric field of -0.07 to -0.14V/cm biased away from the microchannel plates used for detection. This field was used in contrast to our previous implementations of PFI-ZEKE in order to mitigate signals from electrons directly ejected from molecules that were not excited into the high-*n* Rydberg states. The field slightly depressed the NdO^+ ionization energy compared to the field-free configuration, but did so within experimental error. Between 0.7μs and 1.2μs after the laser interaction with the molecular beam the repeller plate was pulsed to -7.5V, providing a total electric field of -1.8 V/cm that ejected the high-*n* Rydberg electrons towards the detector. The signal was demonstrated to belong to NdO^+ as it was not present when the pump laser was not tuned to the NdO transition.

Results

The initial search for the IE of NdO was guided by Ackermann et al.'s[7] value of 4.97(10) eV. As this was a relatively low energy we began by working with low energy pump transitions, so that the probe laser wavelengths would fall in a range that was convenient for the second dye laser. With the pump laser tuned to the [11.540]3-X(1)4 transition[12] we were unable to observe

two-color ionization within the expected energy range. Signals were first observed for probe wavelengths below 303 nm, with a poor signal-to-noise ratio. Fig. 1 shows a PIE scan taken with the pump laser tuned to the R-branch band head of the [11.540]3-X(1)4 transition. The onset of ionization was estimated from this trace by inspection. When the depression of the IE by the local field of the mass spectrometer was taken into account (364 V cm^{-1} shifts by 115 cm^{-1}), the IE was found to be 44426(20) cm^{-1}.

A PFI-ZEKE scan, recorded with the pump laser tuned to the *R*-branch feature of the [11.540]3-X(1)4 transition is shown in Fig. 2. Rotational structure is evident in this trace, but it differs from the structures seen in many of our previous PFI-ZEKE experiments[17,18,24,26]. Typically, we have observed rotational structures where the spacings between successive lines diverge as the energy increases. This reflects the rotational energy level structure of the molecular ion. In contrast, Fig. 2 shows rotational structure where the line spacing diverges with decreasing energy. As discussed below, this follows the energy level pattern of the intermediate excited state ([11.540]3, v=0) with ionization to just the lowest energy rotational level of the ion. Consequently, the IE was defined by the blue edge of the highest energy rotational line. Note that the blue edge was used because it represents the convergence limit of the high-*n* Rydberg states. The data in Fig. 2 yielded an IE of 44427.2(20) cm^{-1} (5.5083 eV), consistent with the field-corrected value obtained from the PIE measurements.

Confirmation that the rotational structure of Fig. 2 was that of the [11.540]3 state was obtained by fitting the line centers (E_J) to the expression

$$E_J = E_0 - BJ(J+1) \qquad (1)$$

Where *J* is the rotational angular momentum quantum number of the [11.540]3 state and E_0 is the ionization energy extrapolated to the hypothetical *J*=0 limit (as Ω=3, *J* cannot be less than 3).

With the *J* assignments indicated in Fig. 2 the fit produced a rotational constant of B=0.338(5) cm^{-1}, in reasonable agreement with the literature value[12] of B=0.3345 cm^{-1}. Alternative rotational numberings yielded larger variances and rotational constants that differed from the literature value by several standard deviations.

Additional confirmation of the assignments was obtained by recording PFI-ZEKE spectra where the frequency of the pump laser was scanned, while the probe laser was fixed on one of the PFI-ZEKE features of Fig. 2. Fig. 3 shows examples of this type of scan. As each PFI-ZEKE peak is produced by a specific $J \rightarrow NdO^+$ transition, a scan of the pump laser produces a spectrum that is dominated by the *P(J+1)*, *Q(J)* and *R(J-1)* rotational lines. Ground state combination differences (e.g., $R(J-1)-P(J+1)=4B''(J+1/2)$, where B''=0.3616 cm^{-1} is the rotational constant for X(1)4[12]) could then be used to determine the *J* values. This independent procedure yielded the same assignments as the fit to Eq. 1 described above.

The IE proved to be considerably higher than the value reported by Ackermann et al.[7] As the next objective was to characterize the first tier of vibronically excited states for the ion, the pump laser was tuned to a higher energy intermediate state to provide facile access to the excited states of the ion. The well-characterized [16.740]3-X(1)4 transition of NdO[10,11] was used for this sequence of measurements. As a check for consistency, PIE and PFI-ZEKE scan recorded using this pump transition yielded an IE value in agreement with the results obtained using [11.540]3 as the intermediate state. The rotational structure of the PFI-ZEKE origin band was similar to that of Fig. 2, and fitting to the rotational energy levels (Eq. 1) yielded a rotational constant that agreed with the reported constant for the [16.740]3 state.

The extended PFI-ZEKE spectrum for NdO^+ exhibited 30 vibronic states in the energy range from the origin band to 5200 cm^{-1} above the IE. A survey scan of the 0 – 2500 cm^{-1} region

is presented in Fig. 4. The electronic state assignments shown in Fig. 4 were derived from the predictions of ab initio calculations given in Table 2. Vibrational progressions with energy intervals near 890 cm^{-1} were easily recognized in this sweep. Band origins and vibrational constants derived from the PFI-ZEKE data are listed in Table 3.

There was some notable variation in the rotational structures of the PFI-ZEKE bands. While the vibrationally excited levels of the X(1)4.5 state had much the same rotational structure as the origin (v=0) band, the structure for (1)3.5 was of the more commonly encountered form, with the line spacings diverging to higher energies. Spectra recorded by scanning the pump laser, with the probe laser fixed on a PFI-ZEKE feature confirmed that the structure of the (1)3.5 bands was due to a short progression of the molecular ion rotational states, beginning with J^+=3.5 Each of these traces showed *P(J+1), Q(J) and R(J-1)* lines where the most intense line was associated with the transition where $J^+=J$-0.5. For example, with the probe laser tuned to J^+=3.5 the most intense line was *R(4)* while the detection of J^+=5.5 resulted in the *P(6)* line being most intense. Higher energy vibronic states in the PFI-ZEKE spectrum had more complex rotational structures where both the intermediate state and molecular ion rotational levels were active in the spectrum. As only a few rotational lines of the ion were observed, with widths close to 2 cm^{-1}, the rotational constant defined by these data had large error limits (B^+=0.41(5) cm^{-1}).

Discussion and Conclusions

The present determination of the IE for NdO established a value that is 0.54 eV higher than the result of Ackermann et al.[7] As noted in the introduction, it is likely that this discrepancy can be traced to thermal excitation of NdO in the earlier determination. Ackermann et al.[7] used thermal vaporization of Nd sesquioxide at a temperature of 2200 K to generate gas phase NdO.

The revised IE for NdO can be used to evaluate the bond dissociation energy of NdO via the relationship

$$D_0(NdO) = D_0(NdO^+) + IE(NdO) - IE(Nd)$$

As $IE(Nd)$ is known (5.5250 eV) and $D_0(NdO^+)$ has been carefully reevaluated by Armentrout at al.[27] (7.28(10) eV), a dissociation energy of $D_0(NdO)$=7.26(10) eV is defined by these data. This is in good agreement with the previously recommended value of 7.18(8) eV[28]. The difference between $IE(NdO)$ and $D_0(NdO)$ establishes that the Nd+O associative ionization reaction is exothermic by 1.76(10) eV. Although this exothermicity is lower than earlier estimates, it is confirmed that Nd is still a promising candidate for atmospheric release experiments.

PFI-ZEKE measurements revealed a pattern of low-energy electronically excited states that was in agreement with the qualitative predictions of LFT models. All of the states observed could be correlated with the $Nd^{3+}(4f^3, {}^4I)O^{2-}$ configuration, an interpretation that was supported by the narrow range of ω_e constants associated with these states[13,17] (c.f., Table 3). From the data in Table 3 it can also be seen that the energy spacing between the Ω=J_a=(1)5.5 and Ω=J_a=(1)4.5 levels (1840 cm^{-1}) is very close to the atomic free ion $^4I_{5.5}$-$^4I_{4.5}$ interval of 1880 cm^{-1} (ref.[22]). This demonstrates the near conservation of the spin-orbit coupling constant.

Another interesting point of comparison between NdO^+ and UO^+ is the magnitude of the ligand-induced splitting of the J_a=4.5 sub-levels. The range of molecular states (Ω=4.5 to 0.5) spans 1719 cm^{-1} for NdO^+ and 1325 cm^{-1} for UO^+. The slightly larger perturbation for NdO^+ may be a consequence of the smaller internuclear distance of 1.74 Å, as compared to R_e=1.80 Å for UO^+. Ionization of both NdO and UO involves the removal of an electron from the outermost metal-centered s-orbital, and the difference between the atomic and molecular IE's reveals the

effect that the removal of this electron has on the bonding. These energy differences are -0.015 and -0.163 eV, corresponding to rather small increases in the bond strength on ionization. This suggests that the s-electrons are essentially non-bonding, but they do influence the equilibrium properties. On ionization the vibrational frequencies increase and the bond lengths shorten for both NdO/NdO^+ and UO/UO^+.

The rotational structures of the PFI-ZEKE bands were unusual and worthy of some comment. As described above, transitions to the X(1)4 state yielded structure that reflected ionization from a range of intermediate state *J*-levels to just the lowest energy rotational state of the ion (J^+=4.5). The participation of multiple intermediate state levels is reasonable given that the pump laser was tuned to the unresolved *R*-branch band head. The probe-scan PFI-ZEKE spectrum had contributions from $J\geq5$ which is expected for R-branch excitation from an Ω=4 ground state. The fact that levels with $J^+>4.5$ did not appear in the PFI-ZEKE spectrum indicates that the high-*n* Rydberg states that converge to these levels are not long-lived. It seems that these levels undergo rapid auto-ionization by means of a rotational channel coupling mechanism. In contrast, the PFI-ZEKE band of the (1)3.5 state was dominated by transitions to the J^+=3.5, 4.5 and 5.5 levels. Signals from higher angular momentum states were below the noise level, suggestive of the opening of rotationally mediated auto-ionization channels. For higher energy states the variation in the auto-ionization rates produced more complex structures with contributions from both the *J* and J^+ manifolds.

The energy levels for NdO^+ predicted by Krauss and Stevens[16] are compared with the experimental results in Table 2. Here it can be seen that the energy ordering of the states was correct, but both the ligand field splitting and spin-orbit coupling contributions to the energy were underestimated. The weaker ligand field splitting can be partially explained by the fact that

the internuclear separation was fixed at distance of 1.85 Å, which is greater than R_e. Comparison of the results from the present MRCI-SO calculations with the experimental data is also facilitated by Table 2. Overall the agreement is improved, but the ligand field and spin orbit interaction energies are still underestimated. Comparison of the predicted free-ion energies of Table 1 with the Ω=J_a molecular levels of Table 2 shows that the former are only slightly perturbed in the molecule. Hence, the disagreement with the experimental spin-orbit interval is due to inadequate treatment of the spin-orbit coupling, rather than a model-dependent overestimation of the participation of the 4f orbitals in covalent bonding. The cause for the underestimation of the ligand field splitting is more difficult to identify. The simplest interpretation is that the calculations do not fully recover the charge separation due to limitations of the basis set. In future studies it will be of interest to see if this defect can be reduced by adding customized diffuse basis functions.

References

1. S. G. Ard, N. S. Shuman, O. Martinez, M. T. Brumbach, and A. A. Viggiano, J. Chem. Phys. **143**, 204303/1 (2015).
2. N. S. Shuman, D. E. Hunton, and A. A. Viggiano, Chem. Rev. **115**, 4542 (2015).
3. R. G. Caton, T. R. Pederson, R. T. Parris, K. M. Groves, P. A. Bernhardt, and P. S. Cannon, presented at the American Geophysical Union, Fall Meeting, 2013.
4. C. S. Stokes and W. J. Murphy, High altitude chemical release systems for project BIME (Brazilian Ionospheric Modification Experiments), project IMS (Ionospheric Modification Studies), project PIIE (Polar Ionospheric Irregularities Experiment), and project Polar Arcs Franklin Research Center, 1987.
5. M. F. Larsen, I. S. Mikkelsen, J. W. Meriwether, R. Niciejewski, and K. Vickery, J. Geophys. Res. **94**, 17235 (1989).
6. R. M. Cox, J. S. Kim, P. B. Armentrout, J. Bartlett, R. A. Van Gundy, M. C. Heaven, S. G. Ard, J. J. Melko, N. S. Shuman, and A. A. Viggiano, J. Chem. Phys. **142**, 134307/1 (2015).
7. R. J. Ackermann, E. G. Rauh, and R. J. Thorn, J. Chem. Phys. **65**, 1027 (1976).
8. L. A. Kaledin and E. A. Shenyavskaya, Opt. Spektrosk. **47**, 1015 (1979).
9. L. A. Kaledin, E. A. Shenyavskaya, and I. Kovacs, Acta Phys. Hung. **54**, 189 (1983).
10. C. Linton, C. Effantin, P. Crozet, A. J. Ross, E. A. Shenyavskaya, and J. d'Incan, J. Mol. Spectrosc. **225**, 132 (2004).
11. C. Linton, T. Ma, H. Wang, and T. C. Steimle, J. Chem. Phys. **129**, 124310/1 (2008).
12. E. A. Shenyavskaya, A. Bernard, and J. Verges, J. Mol. Spectrosc. **222**, 240 (2003).
13. R. W. Field, Ber. Bunsenges. Phys. Chem. **86**, 771 (1982).

14. P. Carette and A. Hocquet, J. Mol. Spectrosc. **131**, 301 (1988).

15. A. R. Allouche, M. Aubert-Frecon, and S. Y. Umanskiy, J. Chem. Phys. **124**, 184317/1 (2006).

16. M. Krauss and W. J. Stevens, Mol. Phys. **101**, 125 (2003).

17. V. Goncharov, L. A. Kaledin, and M. C. Heaven, J. Chem. Phys. **125**, 133202/1 (2006).

18. M. C. Heaven, Phys. Chem. Chem. Phys. **8**, 4497 (2006).

19. R. Tyagi, Z. Zhang, and R. M. Pitzer, J. Phys. Chem. A **118**, 11758 (2014).

20. W. T. Carnall and H. M. Crosswhite, Report No. ANL-84-90, 1984.

21. L. A. Kaledin, J. E. McCord, and M. C. Heaven, J. Mol. Spectrosc. **164**, 27 (1994).

22. J.-F. Wyart, A. Meftah, W.-U. L. Tchang-Brillet, N. Champion, O. Lamrous, N. Spector, and J. Sugar, J. Phys. B At., Mol. Opt. Phys. **40**, 3957 (2007)

23. H.-J. Werner, P. J. Knowles, G. Knizia, F. R. Manby, and M. Schuetz, Wiley Interdiscip. Rev. Comput. Mol. Sci. **2**, 242 (2012).

24. V. Goncharov and M. C. Heaven, J. Chem. Phys. **124**, 064312/1 (2006).

25. M. A. Duncan, Rev. Sci. Instrum. **83**, 041101/1 (2012).

26. M. C. Heaven, B. J. Barker, and I. O. Antonov, J. Phys. Chem. A **118**, 10867 (2014).

27. M. Ghiassee, J-S. Kim, and P.B. Armentrout, J. Chem Phys. submitted (2019).

28. R. J. M. Konings, O. Benes, A. Kovacs, D. Manara, D. Sedmidubsky, L. Gorokhov, V. S. Iorish, V. Yungman, E. Shenyavskaya, and E. Osina, J. Phys. Chem. Ref. Data **43**, 013101/1 (2014).

Table 1. Calculated and observed energy levels for $Nd^{3+}(4f^3, {}^4I)$

J_a	E(Obs)[22]	E(MRCI-SO)	ΔE
4.5	0.0	0.0	0.0
5.5	1897.07	1644	253
6.5	3907.30	3586	321
7.5	5988.50	5828	161

All energies are in cm^{-1} units.

Table 2. Calculated and observed energy levels for $Nd^{3+}(4f^3, {}^4I)O^{2-}$

J_a	Ω	Ref. [16]	MRCI-SO	Observed
4.5	4.5	0	0	0
	3.5	630	1071	1280
	2.5	683	1478	1538
	1.5	780	1485	1624
	0.5	904	1509	1719
5.5	5.5	1291	1630	1840
	4.5	1803	2549	2951
	3.5	1874	2907	3237
	2.5	1957	3054	
	1.5	2126	3069	
	0.5	2192	3078	
6.5	6.5	2733	3444	
	5.5	3265	4314	
	4.5	3298	4704	
	3.5	3459	4881	
	2.5	3538	4927	
	1.5	3541	4943	
	0.5	3729	4950	
7.5	7.5	4366	5454	
	6.5		6342	
	5.5		6847	
	4.5		7033	
	3.5		7085	
	2.5		7099	
	1.5		7099	
	0.5		7115	

All energies are in cm^{-1} units.

Table 3. Observed vibronic states and vibrational constants of NdO^+

State	v^+	$T_{0,v+}$	ω_e	$\omega_e\chi_e$
X(1)4.5	0	0	892.4(15)	1.3(2)
X(1)4.5	1	890.3(20)		
X(1)4.5	2	1775.1(20)		
X(1)4.5	3	2663.1(20)		
X(1)4.5	4	3544.0(20)		
X(1)4.5	5	4422.9(20)		
(1)3.5	0	1280.2(20)	892.9(35)	2.6(8)
(1)3.5	1	2169.3(20)		
(1)3.5	2	3049.3(20)		
(1)3.5	3	3928.0(20)		
(1)2.5	0	1537.7(20)	889.0(26)	1.5(5)
(1)2.5	1	2422.4(20)		
(1)2.5	2	3308.0(20)		
(1)2.5	3	4184.0(20)		
(1)2.5	4	5062.3(20)		
(1)1.5	0	1623.7(20)	890.3(1)	
(1)1.5	1	2514.4(20)		
(1)1.5	2	3405.2(20)		
(1)1.5	3	4296.3(20)		
(1)0.5	0	1719.1(30)	880(3)*	
(1)0.5	1	2596.4(30)		
(1)0.5	2	3471.0(30)		
(1)0.5	3	4362.0(30)		
(1)5.5	0	1840.1(20)	(894)	
(1)5.5	1	2734.7(20)		
(2)4.5	0	2950.8(20)	(894)	
(2)4.5	1	3845.2(20)		
(2)3.5	0	3237.6(20)	892.9(35)	2.6(9)
(2)3.5	1	4127.9(20)		
(2)3.5	2	5013.1(20)		

Energies and vibrational constants are given in cm^{-1} units

* Due to the low intensities and higher uncertainties of the band centers, the vibrational intervals were used to define we with $\omega_e x_e$ held at zero.

Figure captions

1. Photoionization efficiency scan for NdO. The pump laser was tuned to the *R*-branch band head of the [11.540]3-X(1)4 transition. The arrow indicates the estimated ionization threshold in the presence of an electric field of 364 V cm^{-1}.

2. Probe-scan PFI-ZEKE spectrum for NdO. The pump laser was tuned to the *R*-branch band head of the [11.540]3-X(1)4 transition. Band head excitation was used as it gave better signal-to-noise rations as compared to excitation of resolved *P*-branch lines. The numbers given above each peak are the rotational quantum numbers of the NdO [11.540]3 intermediate state.

3. Pump-scan PFI-ZEKE spectra for NdO. For each trace the probe laser was tuned to a specific peak of the spectrum shown in Fig. 2. The pump laser was then scanned through the rotational lines of the [11.540]3-X(1)4 transition. The Q-line numbering indicates the intermediate rotational level of the PFI-ZEKE transition.

4. Probe-scan PFI-ZEKE survey spectrum. The pump laser was tuned to the R-branch band head of the [16.738]3-X(1)4 transition. The energy scale is relative to the IE.

Figure 1

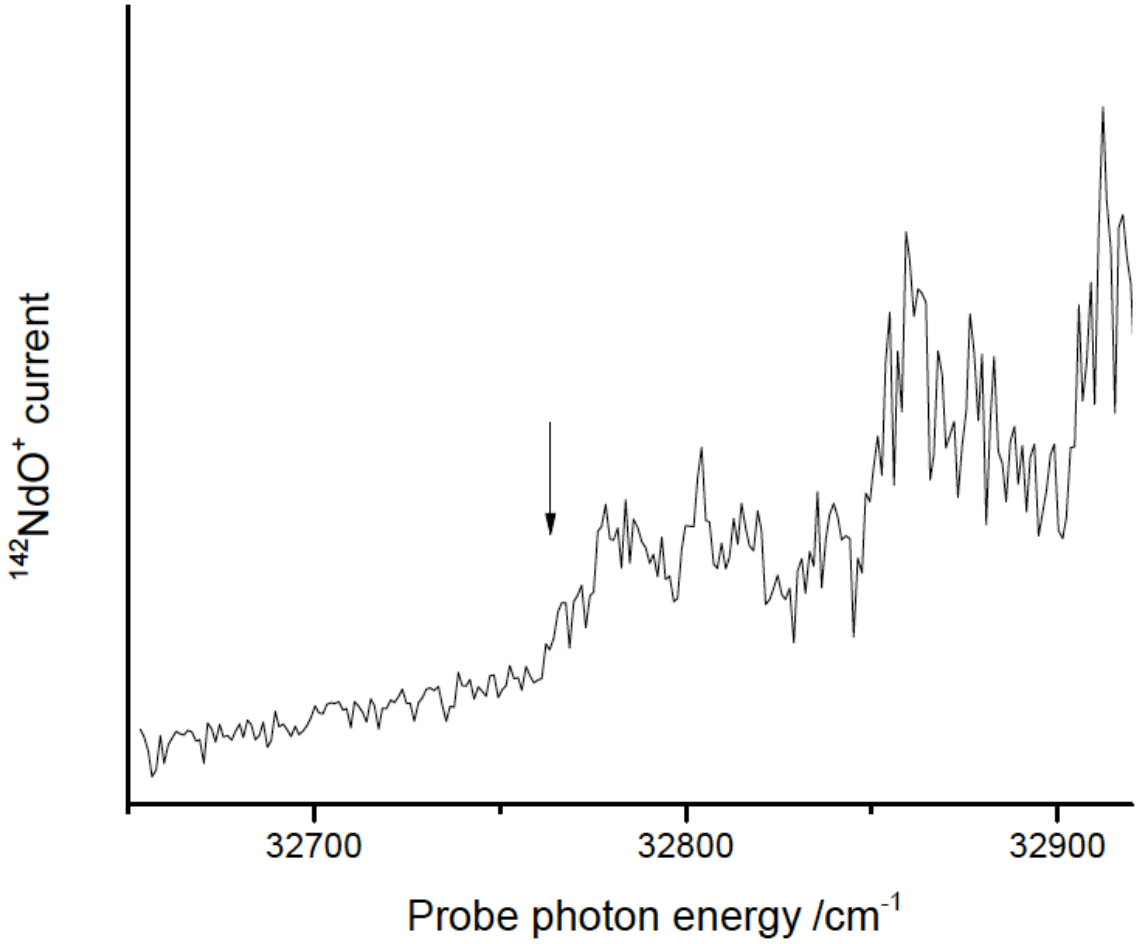

Figure 2

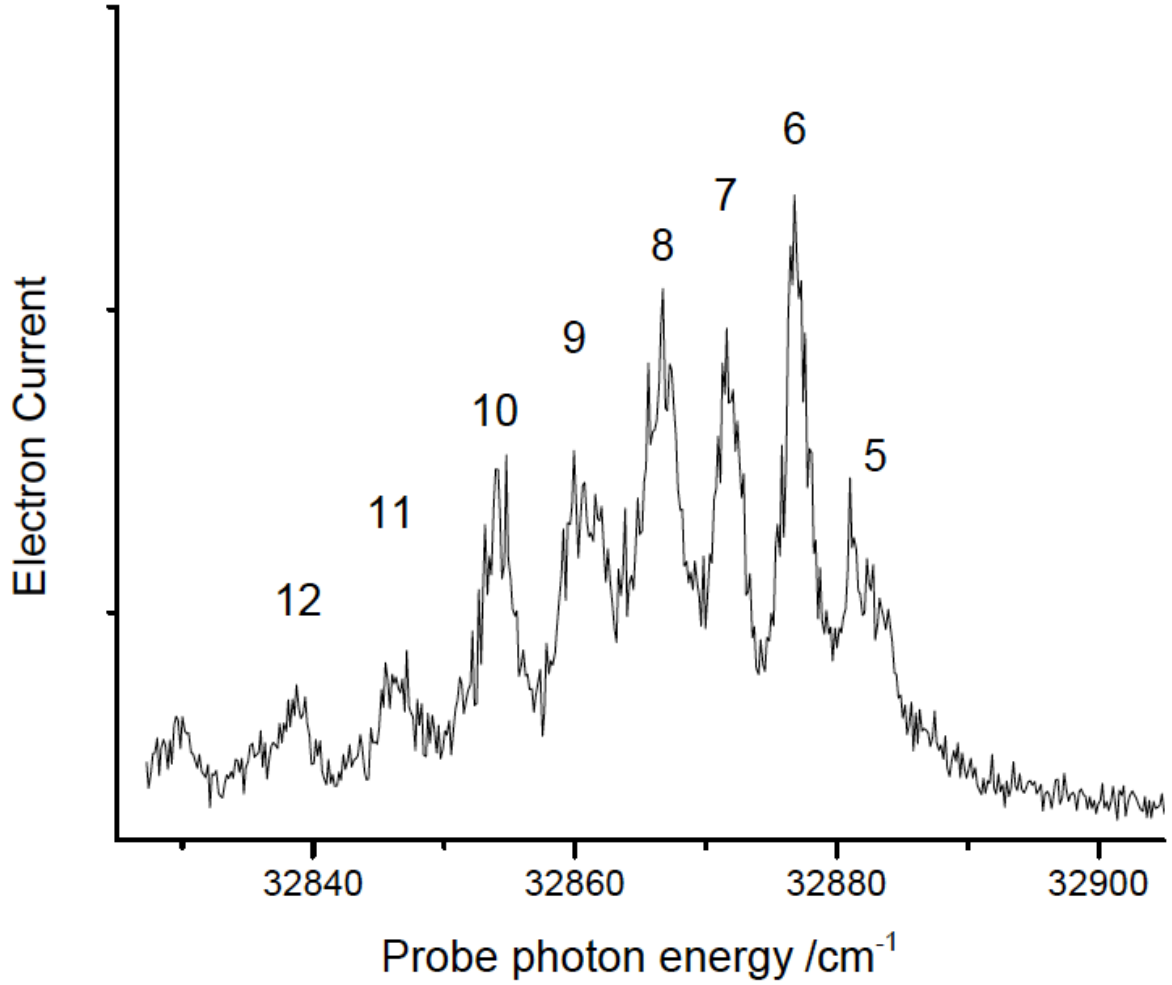
Electron Current
12
11
10
9
8
7
6
5
32840
32860
32880
32900
Probe photon energy /cm-1

Figure 3

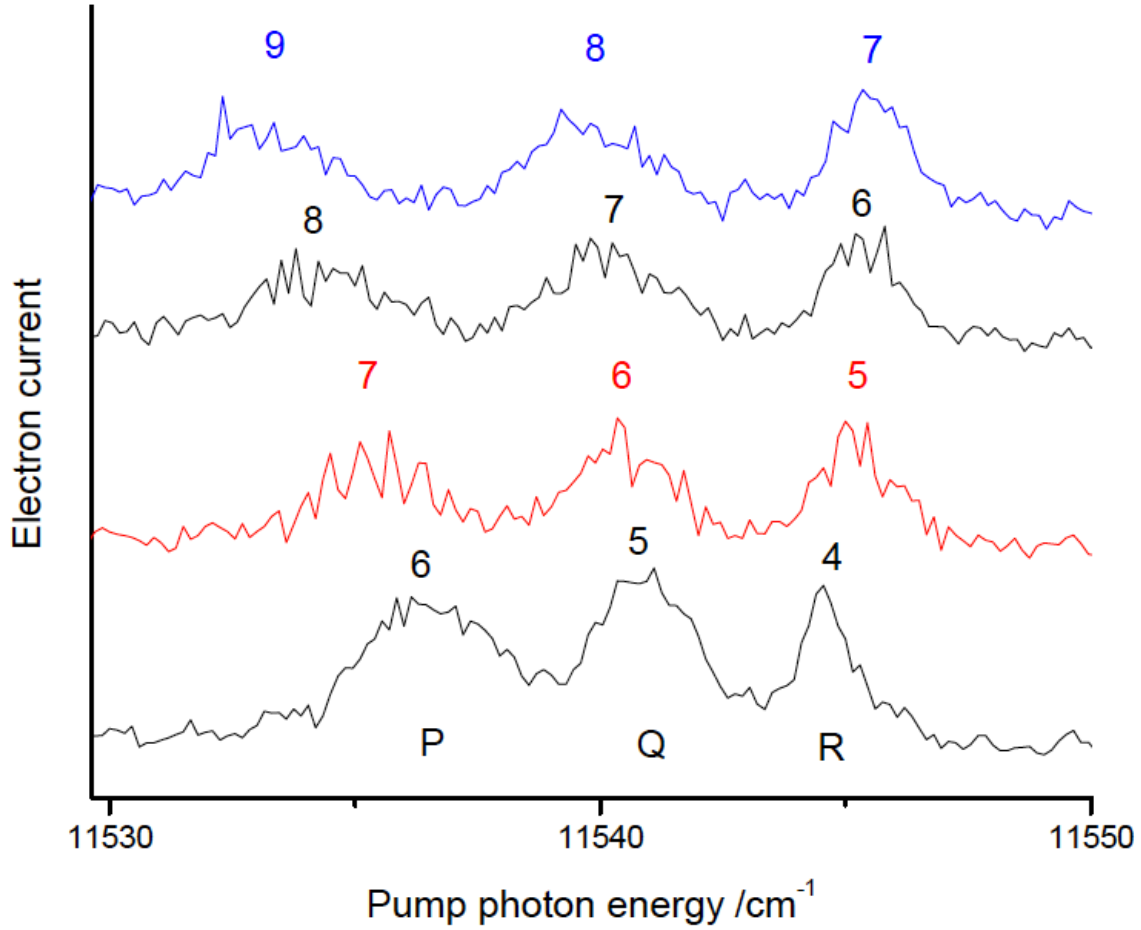
9
8
7
8
7
6
7
6
5
6
5
4
P
Q
R
Electron current
11530
11540
11550
Pump photon energy /cm-1

Figure 4

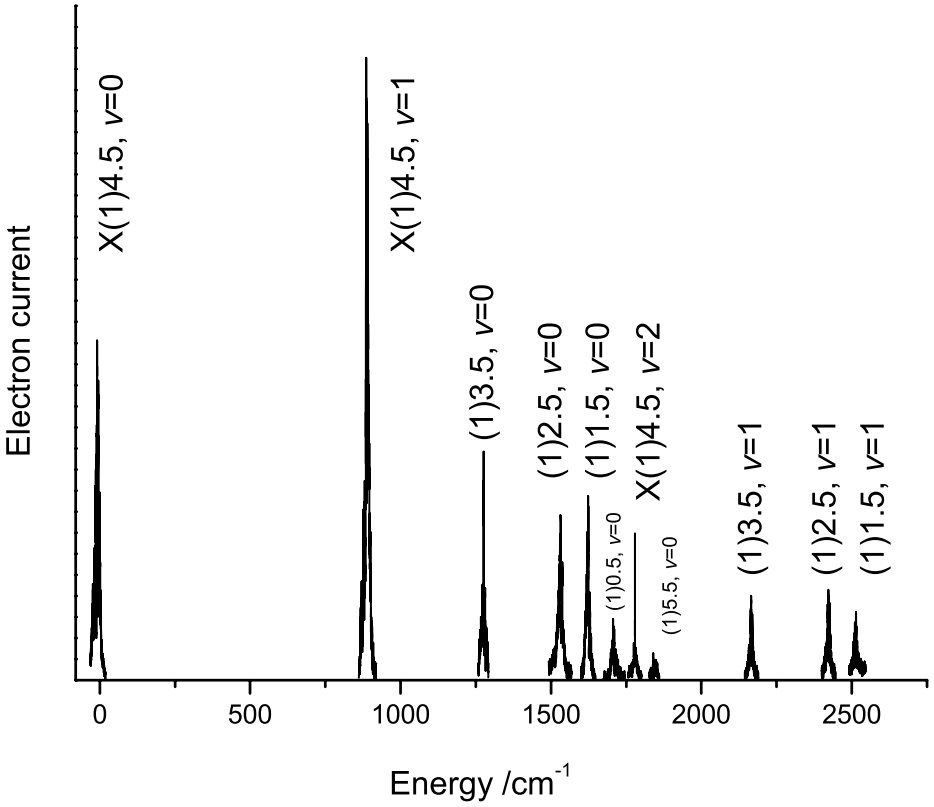
Electron current
X(1)4.5, v=0
X(1)4.5, v=1
(1)3.5, v=0
(1)2.5, v=0
(1)1.5, v=0
(1)0.5, v=0
X(1)4.5, v=2
(1)5.5, v=0
(1)3.5, v=1
(1)2.5, v=1
(1)1.5, v=1
0
500
1000
1500
2000
2500
Energy /cm-1